Energy & Environmental Science

ROYAL SOCIETY OF CHEMISTRY

PAPER

View Article Online
View Journal

Cite this: DOI: 10.1039/d4ee02208d

An all-in-one free-standing single-ion conducting semi-solid polymer electrolyte for high-performance practical Li metal batteries†

Jinping Zhang,[ac] Jie Zhu,[ac] Ruiqi Zhao,[ac] Jie Liu,[ac] Xingchen Song,[ac] Nuo Xu,[ac] Yansong Liu,[ac] Hongtao Zhang,*[ac] Xiangjian Wan,[abc] Yanfeng Ma,[ac] Chenxi Li[ac] and Yongsheng Chen *[abc]

Single-ion conducting polymer electrolytes, characterized by effective Li^+ transport and dendrite mitigation, are emerging as promising candidates for the highly demanded lithium metal batteries. However, despite the promise, their current ionic conductivity and Li^+ transference number fall short of application requirements. Herein, we have developed a free-standing single-ion conducting semi-solid polymer electrolyte (PBSIL), engineered through the synergistic interaction between anion acceptors and solvated ionic liquids. This innovative chemical synergy significantly enhances the complete dissociation of lithium salts while immobilizing anions, thus facilitating rapid Li^+ transport. As a result, the PBSIL electrolyte exhibits enhanced ionic conductivity of 8.0×10^{-4} S cm^{-1}, and an improved Li^+ transference number of 0.75. These features effectively mitigate concentration polarization and dendrite growth, ensuring long-term cell stability. Moreover, Li|PBSIL|$LiNi_{0.8}Co_{0.1}Mn_{0.1}O_2$ cells demonstrate an ultra-long cycle life of 1300 cycles, with a high discharge capacity of 183 mA h g^{-1} and excellent capacity retention of 75%. Additionally, PBSIL has been successfully integrated for the first time into the production of winding-processed semi-solid state cylindrical and *Z*-stacked pouch lithium metal batteries. Through the synergistic regulation of Li^+ transport and anion immobilization, PBSIL provides an effective design strategy for free-standing semi-solid polymer electrolytes, showcasing superior electrochemical performance and contributing to the development and industrialization of long-cycling lithium metal batteries.

Received 21st May 2024,
Accepted 16th August 2024

DOI: 10.1039/d4ee02208d

rsc.li/ees

Broader context

Single-ion conducting semi-solid polymer electrolytes (SICPEs) are highly valued in the development of high-voltage solid-state Li metal batteries (LMBs) due to their high Li^+ transference number, which can effectively mitigate dendrite growth and improve practical performance. However, SICPEs still face challenges in achieving rapid Li^+ transport, particularly when integrated with mass production and conventional battery fabrication processes. Herein, we developed a roll-to-roll processable, free-standing single-ion conducting semi-solid polymer electrolyte (PBSIL) with precise regulation of Li^+ transport and anion immobilization through the synergistic interaction of anion acceptor and solvate ionic liquid. As a result, the optimized PBSIL, with enhanced Li^+ migration and anion immobilization, significantly inhibits Li dendrite growth and exhibits ultra-long cycle life in Li‖$LiNi_{0.8}Co_{0.1}Mn_{0.1}O_2$ cells. More importantly, PBSIL has been successfully fabricated on a large scale and implemented in the semi-solid state cylindrical and *Z*-stacked pouch LMBs at ambient temperature. Our work demonstrates an effective strategy for regulating Li^+ transport and anion immobilization regulation, paving the way for the development of dendrite-free and long-cycling Li metal batteries. These advancements hold substantial promise for scaling up to industrial-level battery production, marking a significant step forward in the evolution of energy storage technologies.

[a] *The Centre of Nanoscale Science and Technology and Key Laboratory of Functional Polymer Materials, Institute of Polymer Chemistry, College of Chemistry, Nankai University, Tianjin 300071, China*
[b] *State Key Laboratory of Elemento-Organic Chemistry, Nankai University, Tianjin, 300071, China*
[c] *Renewable Energy Conversion and Storage Center (RECAST), Nankai University, Tianjin 300071, China. E-mail: yschen99@nankai.edu.cn, htzhang@nankai.edu.cn*

† Electronic supplementary information (ESI) available. See DOI: https://doi.org/10.1039/d4ee02208d

1. Introduction

Solid-state electrolytes (SSEs) are increasingly recognized for their substantial safety and stability advantages over liquid electrolytes (LEs), making them the most promising approach for the development of high-voltage lithium metal batteries (LMBs).[1–4] The scalable fabrication of practical solid-state

LMBs depends on the choice of SSEs, which determines the processing technologies that can be used for LMBs fabrication.[5,6] Therefore, a major challenge in the industry is the development of large-scale, free-standing SSEs that can be produced cost-effectively through roll-to-roll continuous production processes. This is crucial for achieving mass production and practical application of solid-state LMBs.[7,8] Compared to inorganic electrolytes, which suffer from poor mechanical/interfacial properties and challenges in scaling up production, polymer electrolytes (PEs) with flexibility and roll-to-roll scale-up processability have been argued as one of the most promising systems to be compatible with commercial cylindrical, prismatic, and pouch cell structures.[9] Importantly, high ion conductivity ($\sigma > 10^{-4}$ S cm^{-1}) and lithium ion transference number ($t_{Li+} \approx 1$) should also be achieved for PEs to meet the performance including practical and stability requirements.[10,11]

It is widely recognized that enhancing Li^+ migration while simultaneously inhibiting anion transport can significantly improve lithium ion conductivity of PEs, thereby boosting their practical performance in high-voltage LMBs.[12,13] Single-ion conducting polymer electrolytes (SICPEs), characterized by anions covalently bonded to the polymer or immobilized by anion acceptors to achieve high t_{Li+} value (close to unity), have generated considerable attention.[14–19] In comparison to polymers with covalently linked anions, SICPEs incorporating anion acceptors provide multiple advantages, including convenient synthesis, low cost, and excellent electrochemical stability, making them particularly suitable for high-performance applications.[13,20–24] Nevertheless, SICPEs prepared without plasticizers still suffer from low room-temperature (RT) ionic conductivity due to the high crystallinity of the polymer chains and inadequate dissociation of Li salts, limiting their application in LMBs.[25–27] Additionally, the high volatility and flammability of conventional LEs used as plasticizers drastically reduce the thermal stability of PEs, thereby constraining their viability for large-scale industrial processes.[28] In response to these challenges, the development of solvate ionic liquids (SILs) has been identified as a promising solution. Characterized by low volatility, nonflammability, superior electrochemical stability, and low viscosity, SILs effectively improve the ionic conductivity and safety of PEs while avoiding the disadvantage of volatilization associated with traditional LEs and the high viscosity of ionic liquid.[29,30] Their unique properties have led to the proposal of several new PEs incorporating SILs, showcasing their potential to replace traditional plasticizers.[31–35] Therefore, it is reasonable to consider SILs as a promising plasticizer for SICPEs to achieve large-scale production and excellent electrochemical performance in high-voltage LMBs.

In this work, we have developed an all-in-one free-standing single-ion conducting semi-solid polymer electrolyte (named as PBSIL), leveraging the synergistic interaction between anion acceptor (Borate ester) and SIL composed of [Li(G_4)][TFSI] (G_4: tetraglyme). This design capitalizes on the Lewis acidity of anion acceptor to endow PBSIL with enhanced t_{Li+} and weakened ionic association of LiTFSI. Simultaneously, the solvation interaction between G_4 and Li^+ in SIL promotes the complete dissociation of lithium salts, facilitating Li^+ mobility. Therefore, PBSIL exhibits a high ionic conductivity of 8.0×10^{-4} S cm^{-1} at 25 °C, a high t_{Li+} of 0.75, and a wide electrochemical window (5.3 V *versus* Li/Li$^+$), effectively suppressing Li dendrite growth.[14,23,36–38] Thus, due to these exceptional electrochemical properties of PBSIL, high-voltage Li|PBSIL|$LiNi_{0.8}Co_{0.1}Mn_{0.1}O_2$ (NCM811) cells deliver an ultra-long cycle life of 1300 cycles with an excellent capacity retention of 75%, which is one of the best results reported to date for free-standing polymer electrolytes. More importantly, our developed PBSIL have been successfully implemented in both semi-solid state cylindrical and *Z*-stacked pouch cells operated at ambient temperature, highlighting its substantial promise for practical industrial applications. This work underscores the crucial role of fine-tuning the chemical interaction between anion acceptor and SIL in developing dendrite-free and long-cycling Li metal batteries and offering significant advancements for application in industrial level.

2. Results and discussion

PBSIL was synthesized *via* the free radical polymerization of unsaturated C=C bonds under UV irradiation (Scheme 1). Initially, a homogenous precursor solution was prepared, composed of plasticizer (SIL, [Li(G_4)][TFSI]), anion acceptor (Borate ester, AAPE), crosslinker (PETA), matrix material (PVDF-HFP), and photoinitiator (HMPP). Different designed ratios (Tables S1 and S2, ESI†) were studied to prepare a series of solutions. These solutions were then drop-casted onto a flat glass dish and exposed to UV light, which initiated the radical polymerization of C=C bonds (more details are given in the Experimental section, ESI†). Subsequently, the optimized all-in-one semi-solid polymer electrolyte membrane with a thickness of 51 μm was obtained after vacuum drying for 24 h at 60 °C (the inset in Fig. 1a). Furthermore, the successful fabrication of a large-size polymer membrane highlights the feasibility of employing roll-to-roll manufacturing for PBSIL. This process underscores PBSIL's potential as a promising candidate for semi-solid state, winding-processed cylindrical and *Z*-stacked pouch cells (Fig. 1a and Fig. S1, ESI†).

Fourier transform infrared spectroscopy (FTIR) and proton nuclear magnetic resonance (^{1}H-NMR) were used to verify the successful polymerization of monomers in the PBSIL samples (Fig. S2 and S3, ESI†), indicating excellent radical polymerization activity of anion acceptor AAPE.[38,39] To achieve the best balance between mechanical properties, ionic conductivity, and t_{Li+}, the precursor compositions were systematically optimized (Table S1, ESI†). Moreover, the ratio of anion acceptor to SIL was carefully adjusted to regulate the anion acceptor-SIL synergistic interaction, achieving a high ionic conductivity (up to 9.2×10^{-4} S cm^{-1}) and t_{Li+} (up to 0.86) (Fig. 1b, Table S2, and Fig. S4, ESI†). The optimized PBSIL with 15 wt% AAPE, demonstrating both high ionic conductivity (8.0×10^{-4} S cm^{-1}) and t_{Li+} (0.75) (Fig. 1b and c), was selected for the further investigations. In contrast, the electrolyte membrane prepared without

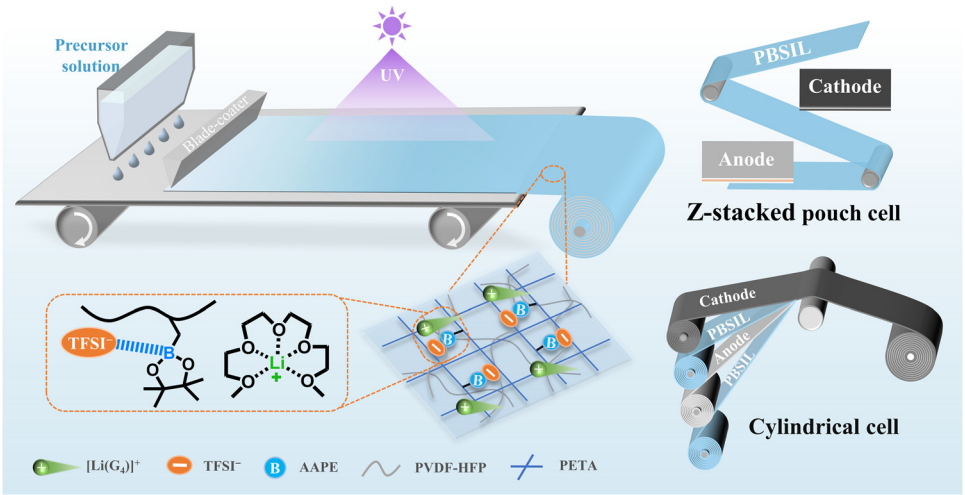

Scheme 1 Schematic illustration of the PBSIL membrane fabrication process *via* photoinitiated free radical polymerization and the scalable manufacturing process for cylindrical and pouch cells.

AAPE (denoted as PSIL) exhibits significantly lower ionic conductivity of 4.2×10^{-4} S cm^{-1} and t_{Li+} of 0.49 (Fig. 1b and Fig. S5, ESI†). To explore the mechanism of the high t_{Li+} of PBSIL, the interaction between AAPE and anion was further studied by density functional theory (DFT) calculations. The adsorption energy of F and O atoms (in TFSI$^-$) with B atom (in AAPE) are −0.37 and −0.23 eV, respectively, confirming the strong Lewis acid–base interaction between TFSI$^-$ and AAPE.[40,41] Therefore, anion acceptor-SIL synergistic interaction endows PBSIL with abundant free Li$^+$ and immobilized TFSI$^-$, leading to the improved ionic conductivity and t_{Li+}.[19,42,43] The temperature-dependent ionic conductivity was investigated by the Arrhenius equation, indicating a lower activation energy (E_a) of PBSIL (0.27 eV) for Li$^+$ transport than PSIL (0.47 eV) (Fig. 1e and Fig. S6, ESI†). Furthermore, linear sweep voltammetry (LSV) measurements and electrochemical floating analysis were used to investigate the electrochemical stability of PBSIL.[44] Benefiting from the anion acceptor-SIL synergistic interaction, PBSIL reaches a high oxidation potential of 5.3 V (Fig. 1f).[14,32] The result of electrochemical floating analysis

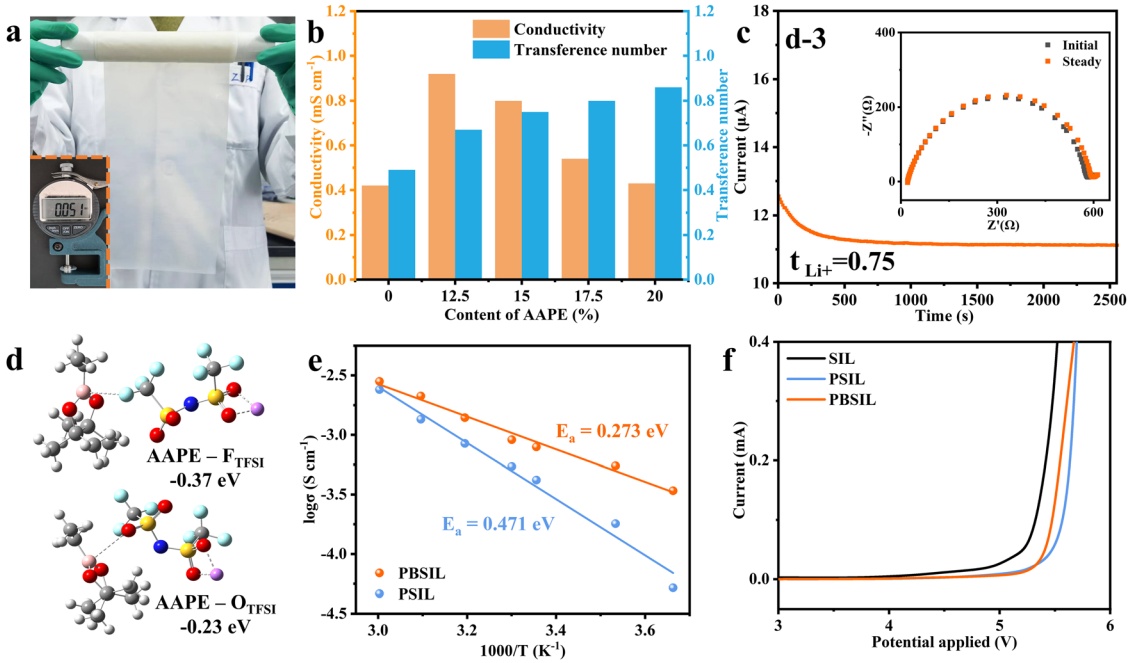

Fig. 1 (a) Optical images of the all-in-one large-size PBSIL membrane and the corresponding electrolyte thickness as inset. (b) Ambient-temperature ionic conductivities and lithium ion transference numbers of PBSIL with varying anion acceptor contents (in weight ratios). (c) Lithium ion transference number of PBSIL. (d) Adsorption energy between TFSI$^-$ and AAPE. (e) Arrhenius plots of PBSIL and PSIL at different temperatures. f) Linear voltammetry curves of SIL, PSIL, and PBSIL.

further indicates a higher oxidation potential (4.9 V) of PBSIL than the control PSIL (4.6 V) (Fig. S7, ESI†). With the electron-deficient center borate, the anion acceptor AAPE has a strong Lewis acid–base interaction with anions, which can promote the dissociation of lithium salt, facilitate anions adsorption to the polymer chains, and induce homogeneous charge dispersion. Thus, it mitigates the anion decomposition and enhances oxidation stability.[13,45] These results demonstrate the potential of PBSIL to partner with high-voltage cathodes to achieve high energy density. In addition, the stress–strain curves of PBSIL demonstrate a tensile strength of 1.18 MPa and high stretchability (maximum strain of 259.9%), ensuring intimate electrolyte/electrode contact and facilitating LMBs assembly (Fig. S8, ESI†).[46,47] Additionally, thermogravimetric analysis also indicates the adequate thermal stability of PBSIL (Fig. S9, ESI†), meeting the operational requirements of practical batteries.

The compatibility of PBSIL with Li metal anode was investigated by measuring the galvanostatic cycling performances of symmetric Li‖Li cells at 0.1 mA cm^{-2}. The Li|PBSIL|Li cell demonstrates the ability to maintain a relatively stable voltage polarization without short-circuiting over 3100 h. In contrast, the control Li|SIL|Li (solvate ionic liquids as electrolyte) and Li|PSIL|Li (polymer electrolyte without anion acceptor AAPE) cells experience short-circuits at 400 h and 1200 h, respectively (Fig. 2a). These results demonstrate the outstanding compatibility and interfacial stability between the PBSIL membrane and lithium metal anode. Moreover, the Li|PBSIL|Li cell exhibits a high critical current density (0.8 mA cm^{-2}) (Fig. S10a, ESI†), which is better than the control PSIL (0.5 mA cm^{-2}) without AAPE (Fig. S10b, ESI†). The surface and cross-sectional morphology of lithium metal electrodes before and after lithium plating/stripping cycling were characterized by scanning electron microscopy (SEM). The cycled Li metal electrode after 50 cycles in the Li|PBSIL|Li cell exhibits a smooth surface and dense deposition layer without obvious thickness increase (406 μm, compared to pristine 400 μm Li) (Fig. 2b, e and Fig. S11, ESI†), demonstrating homogeneous Li deposition and effective inhibition of Li dendrite growth in this system.[48] In sharp

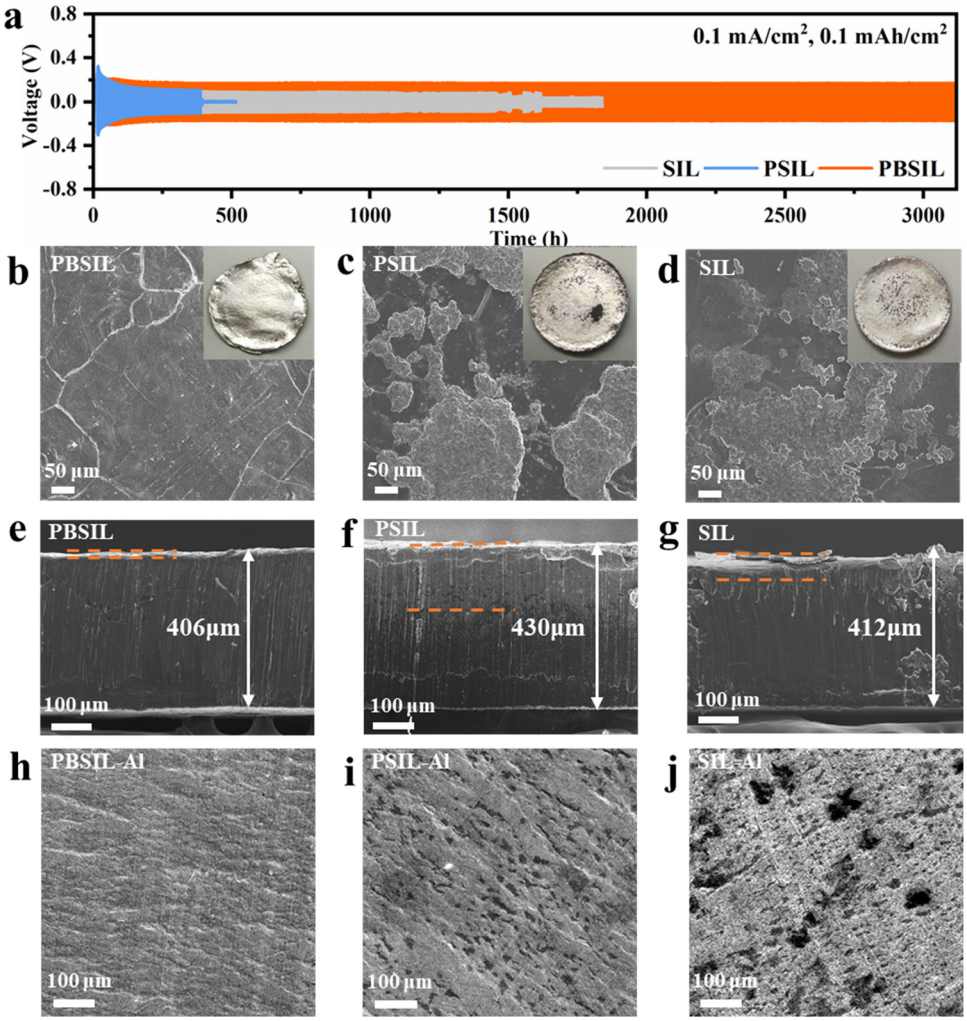

Fig. 2 (a) Galvanostatic plating/stripping profiles of Li‖Li symmetric cells prepared with PBSIL and the two control PSIL and SIL systems. Top-view and cross-sectional SEM images of Li metal electrodes after 50 cycles with (b) and (e) PBSIL, (c) and (f) PSIL, and (d) and (g) SIL. Insets: optical images of the cycled Li metal electrodes. SEM images of Al foil after the chronoamperometry test for 5 h at 5.0 V with (h) PBSIL, (i) PSIL, and (j) SIL.

contrast, the cycled Li metal electrodes obtained from the reference Li|PSIL|Li and Li|SIL|Li cells show clear evidence of mossy and dendritic lithium growth (Fig. 2c, d and Fig. S12, ESI†), along with a considerable increase in thickness to 430 μm and 412 μm, respectively (Fig. 2f and g). These results highlight the loose deposition morphology and inadequate dendrite-suppression capability of these two control systems, reinforcing the effectiveness of PBSIL in enhancing the structural integrity and electrochemical performance of LMBs.

To reveal the mechanism of Li dendrite growth inhibition by PBSIL, the compositions of the solid electrolyte interphase (SEI) on the cycled Li metal electrodes were further studied by X-ray photoelectron spectroscopy (XPS) using Ar ion etching for depth profiling (Fig. S13, ESI†). In the B 1s spectra, the Li–B–O signal at 191.5 eV of PBSIL system is attributed to the AAPE-derived B-rich SEI (Fig. S13a, ESI†),[49] which is regarded as a good ionic conductor with low Li^+ diffusion barrier.[50] In the N 1s spectra, the presence of LiN_xO_y and Li_3N species indicates the decomposition of $TFSI^-$.[51] The SEI from PBSIL system exhibits a reduced intensity of LiN_xO_y and Li_3N peaks, compared with the two control SIL and PSIL systems (Fig. S13b, e and h, ESI†). This indicates that the continuous decomposition of $TFSI^-$ is mitigated in our all-in-one PBSIL system, which benefits from the anion immobilization of AAPE.[51] The presence of Li–B–O and LiN_xO_y, known for their excellent Li^+ conductors, promotes ion conduction and ensures a uniform Li^+ flux distribution at the interface.[52,53] In the F 1s spectra, the distinct LiF and C–F peaks at 684.9 and 688.6 eV, respectively, can be ascribed to the decomposition of PVDF-HFP and $TFSI^-$, indicating a LiF-rich robust SEI layer formed in PBSIL system, which plays a crucial role in inhibiting dendrite growth (Fig. S13c, ESI†).[54] Therefore, the formation of a stable and robust SEI layer in the PBSIL system is instrumental in constructing the dendrite-free Li metal batteries.

In addition, Al current collector corrosion is a significant issue in sulfimide salt-based electrolyte systems, which has severely impeded their widespread application.[55–57] To investigate the anodic behavior of Al in the Li‖Al battery systems, chronoamperometry test and SEM analysis were conducted. The Li‖Al cells were measured by chronoamperometry test for 5 h at 5.0 V, and then the surface morphologies of obtained Al electrodes were examined by SEM. The Li|PBSIL|Al cell exhibits a remarkably decreased anodic corrosion current, and no obvious corrosion has been observed on the Al surface (Fig. 2j). In comparison, the anodic current of the Li|SIL|Al and Li|PSIL|Al control cells significantly increase during the holding time (Fig. S14, ESI†). Furthermore, SEM images of these control cells displayed extensive corrosion damage on the Al surfaces (Fig. 2h and i). These experimental results prove that the anion acceptor-SIL synergistic interaction within our PBSIL electrolyte effectively mitigates Al corrosion, contributing to the long-term cycling performance of high-voltage Li metal batteries.

To further explore the synergistic effect of anion acceptor and SIL on Li^+ migration, the solvation environment around the Li^+ was investigated by molecular dynamics (MD) simulations and high-resolution Li solid state nuclear magnetic resonance (^{7}Li ssNMR) tests. MD simulation snapshots of PSIL (SIL-PETA) and PBSIL (SIL-PETA-AAPE) systems (Fig. 3a and b) provide insights into the interactions between Li^+ and G_4/$TFSI^-$. Radial distribution functions (RDFs) were calculated to obtain detailed information on the statistically averaged structural properties of the ions in these systems. In the control PSIL system, a strong intensity of the $Li–O_{TFSI}$ peak suggests the tight binding of $TFSI^-$ with Li^+. In contrast, within the designed PBSIL system, the peak for $Li–O_{TFSI}$ exhibits a remarkably reduced peak intensity (Fig. 3d), suggesting that $TFSI^-$ is positioned further from Li^+.[31] Furthermore, the binding energy between Li^+ and O atom of $TFSI^-$ is remarkably reduced (−1.36 eV) (Fig. 3f), much lower than that of PSIL system (−2.17 eV) (Fig. 3e). These results suggest that the Li^+-$TFSI^-$ interaction is significantly weakened by the anion acceptor-SIL synergistic interaction, compared to sole solvation of Li^+ in SIL.[21] To confirm the alteration in Li^+-$TFSI^-$ interaction, ^{7}Li ssNMR was utilized to elucidate the changes in the chemical environments of Li^+ within the PSIL and PBSIL polymer electrolytes. The ^{7}Li resonances locate at −0.86 ppm for PBSIL and at −0.91 ppm for the control PSIL (Fig. 3g), respectively. The ^{7}Li resonance for PBSIL shifts to higher frequency corresponding lower electron density around the Li^+, implying weaker Li^+-$TFSI^-$ interaction and more free-moving Li^+, which is consistent with the calculation results.[58,59] In summary, the MD simulation and ^{7}Li ssNMR results conclusively demonstrate that the anion acceptor-SIL synergistic interaction endows our PBSIL system with weakened ionic association of LiTFSI, leading to enhanced Li^+ migration.

Owing to the outstanding electrochemical performance of PBSIL, a Li metal battery with NCM811 cathode was assembled to evaluate the high-voltage LMB performance under a cutoff voltage of 4.3 V. The assembled Li|PBSIL|NCM811 cell exhibits an ultrahigh discharge capacity of 209 mA h g^{-1} at 0.2C, maintaining an impressive capacity retention of 94.4% after 100 cycles at 25 °C (Fig. 4a). In contrast, both Li|SIL|NCM811 and Li|PSIL|NCM811 cells using the two control electrolyte systems deliver significantly lower discharge capacities and worse cycling performance. The surface morphologies of high-voltage NCM811 cathodes after 100 cycles in Li‖NCM811 cells with different electrolytes were characterized by SEM (Fig. S15, ESI†). The cycled NCM811 particles from the Li|PBSIL|NCM811 cell display well-preserved mechanical integrity, whereas the cycled NCM811 particles from the control Li|SIL|NCM811 and Li|PSIL|NCM811 cells show clear intergranular cracking. The structure of cathode electrolyte interphase (CEI) was systematically investigated using in-depth XPS (Fig. S16, ESI†). In the B 1s spectra, the B–O/B–F signal at 191.5 eV of the PBSIL system is attributed to the decomposition of AAPE on the cathode (Fig. S16a, ESI†), indicating enhanced interfacial ion conduction and surface stabilization.[60] In the N 1s spectra, the reduced intensity of LiN_xO_y peaks in PBSIL system suggests that the anion immobilization of AAPE mitigates ongoing decomposition of $TFSI^-$ (Fig. S16b and e, ESI†). In the F 1s spectra, the PBSIL system displays more pronounced LiF (684.9 eV) and B–F (686.7 eV) peaks compared to the PSIL

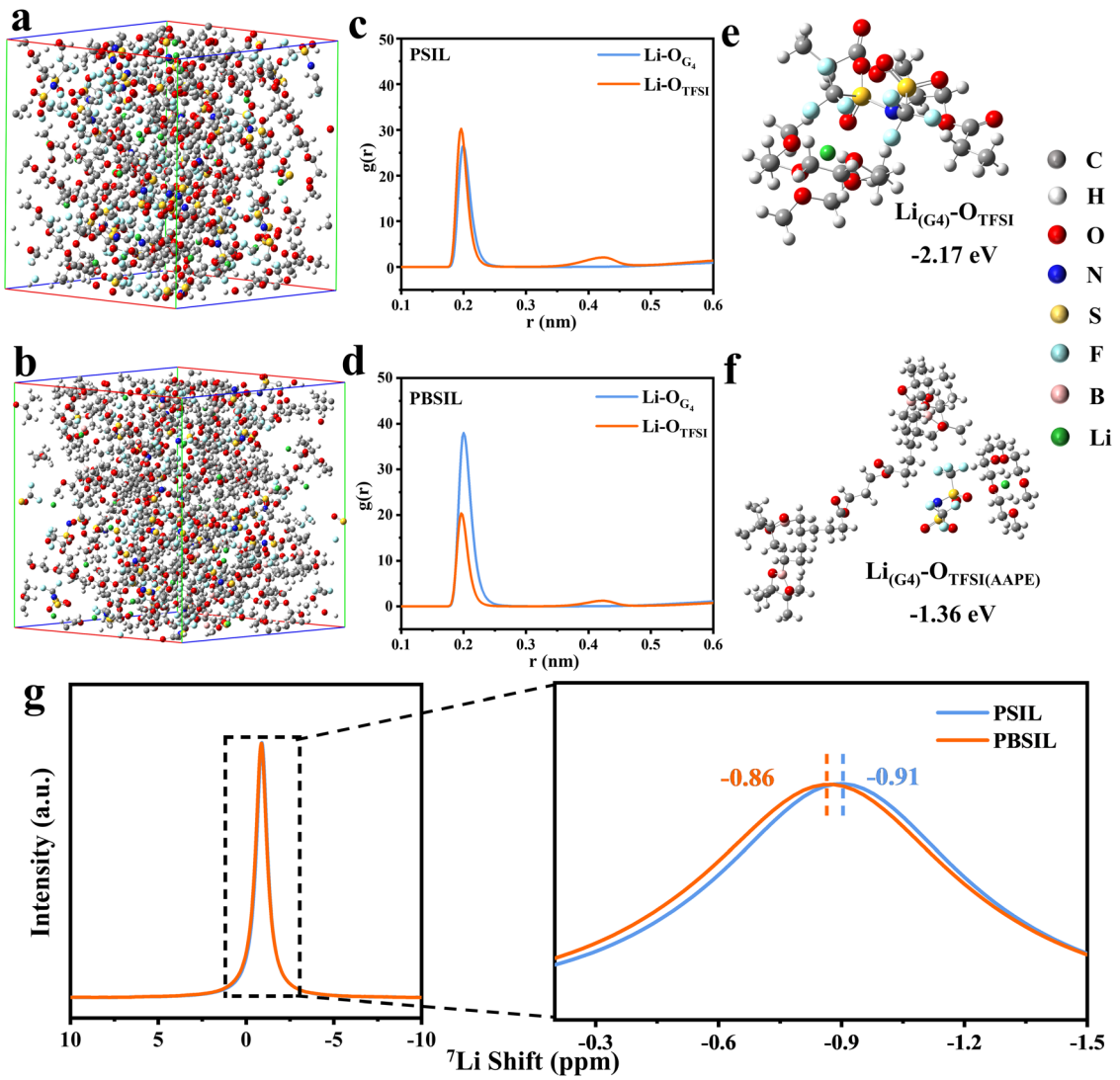

Fig. 3 Molecule dynamics (MD) simulation snapshots of (a) PSIL, (b) PBSIL systems. Radial distribution functions (RDFs) of (c) PSIL, (d) PBSIL systems. Binding energy between Li^+ and O atom of $TFSI^-$ in (e) PSIL, (f) PBSIL systems. (g) ^{7}Li ssNMR spectra of PSIL and PBSIL.

system, indicating the formation of a LiF-rich robust CEI layer that inhibits the oxidative decomposition of electrolyte (Fig. S16c and f, ESI†).

Moreover, high-resolution transmission electron microscopy (HRTEM) was employed to examine the morphology of CEI and the crystal structure of cycled NCM811 cathode in the PBSIL system. A uniform, thin CEI layer (~2.7 nm) and well-retained layer structure, devoid of any rock-salt formation, were observed in the PBSIL system (Fig. S17, ESI†). These observations underscore PBSIL's superior compatibility with high-voltage cathodes and suggest effective suppression of parasitic reactions and electrolyte consumption within the Li|PBSIL|NCM811 cell system.[61,62] Furthermore, during extended cycling evaluation, the Li|PBSIL|NCM811 cell delivers an ultra-long cycle life of 1300 cycles, with an impressive capacity retention of 75% and a high initial discharge capacity of 183 mA h g^{-1} at 0.5C. At a higher rate of 1C, the Li|PBSIL|NCM811 cell achieves a prolonged cycle life of 1500 cycles with an initial discharge capacity of 156 mA h g^{-1} (Fig. S18, ESI†). To the best of our knowledge, these results are among the most impressive results ever reported for free-standing polymer electrolytes (Table S3, ESI†). The Li|PBSIL|NCM811 cell also delivers a prominent rate performance with high specific capacities of 218.4, 208.3, 188.3, 166.4, and 143.4 mA h g^{-1} at 0.1, 0.2, 0.5, 1, and 2C, respectively, far ahead of the reference Li|PSIL|NCM811 cell (Fig. S19, ESI†). Moreover, the impact of electrolyte thickness on battery performance was also investigated through rate performance tests (Fig. S20, ESI†). As a result of increased Li^+ transport distances, Li|PBSIL|NCM811 cells with thicker electrolytes exhibit lower discharge specific capacities and inferior rate performances, demonstrating the importance of controlling electrolyte thickness for optimal cell performance. Owing to the high oxidation stability of PBSIL, the Li|PBSIL|NCM811 cell operating at a cutoff voltage of 4.5 V exhibits an ultrahigh discharge capacity of 215 mA h g^{-1} at 0.2C, with robust cycling stability over 100 cycles (Fig. S21, ESI†).

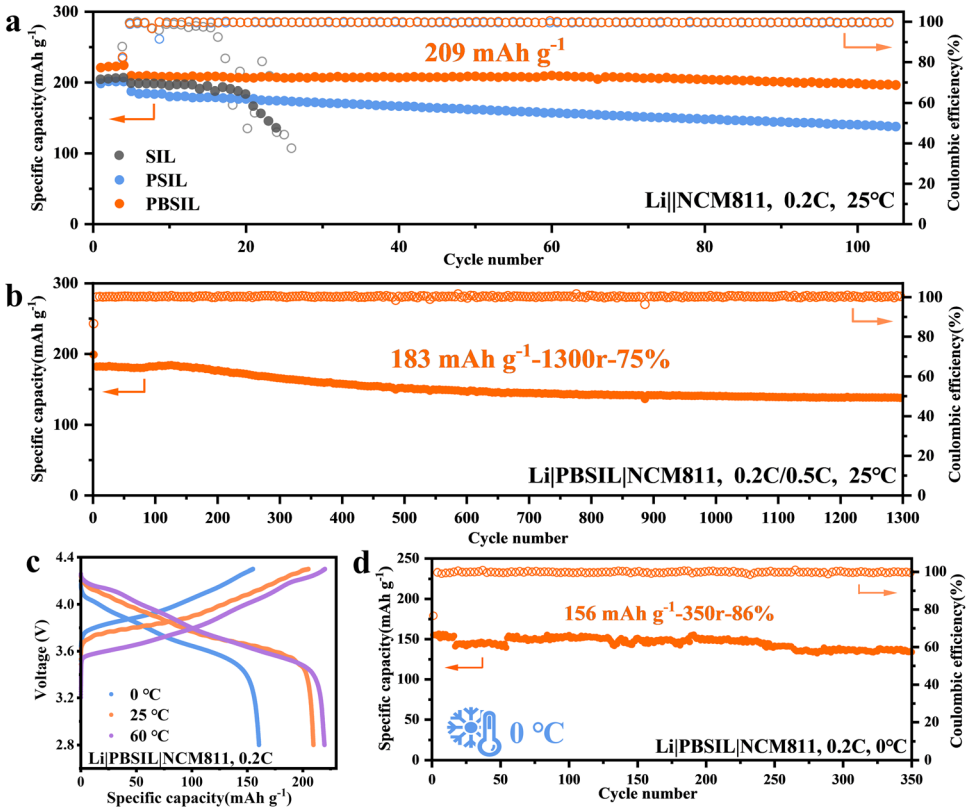

Fig. 4 (a) Cycling performances of Li‖NCM811 cells prepared with PBSIL and the control PSIL and SIL systems at 0.2C. (b) Long-cycling performance of Li|PBSIL|NCM811 cell with charging at 0.2C and discharging at 0.5C. (c) Charge–discharge profiles of Li|PBSIL|NCM811 cell at different temperatures. (d) Cycling performance of Li|PBSIL|NCM811 cell at 0 °C.

In addition, encouraged by the high ionic conductivity and low activation energy of PBSIL, the performance of Li|PBSIL|NCM811 cell was further evaluated across a broad temperature range. At 0 °C and 60 °C, the cells displayed excellent initial discharge capacities of 160 mA h g^{-1} and 219 mA h g^{-1} respectively (Fig. 4c and Fig. S22, ESI†). Furthermore, even at 0 °C, the Li|PBSIL|NCM811 cell exhibits long-cycling stability with a capacity retention of 86% over 350 cycles at 0.2C (Fig. 4d).

Successful electrolyte engineering must accommodate a variety of commercial cathode materials. To this end, the PBSIL electrolyte has been evaluated with different cathode materials, including $LiFePO_4$ (LFP), $LiNi_{0.6}Mn_{0.2}Co_{0.2}O_2$ (NCM622), and Li-rich oxide $Li_{1.2}Mn_{0.54}Co_{0.13}Ni_{0.13}O_2$ (LMCNO), at cutoff voltages of 4.0, 4.3, and 4.6 V, respectively. Owing to the high ionic conductivity and high t_{Li+} of PBSIL, the Li|PBSIL|LFP cell achieves a high capacity of 135 mA h g^{-1}, maintaining excellent capacity retention of 90% after 1000 cycles at 1C (Fig. S23, ESI†), along with superior rate performance (Fig. S24, ESI†). In addition, the Li|PBSIL|NCM622 cell exhibits a high initial discharge capacity of 169 mA h g^{-1} with a capacity retention of 77% after 300 cycles at 0.2C (Fig. S25, ESI†). More notably, benefiting from the superior electrochemical stability of PBSIL, the Li|PBSIL|LMCNO cell operating at a higher charge cutoff voltage of 4.6 V maintains steady operation and display an outstanding discharge capacity of 219 mA h g^{-1} and 95 stable cycles (Fig. S26, ESI†).[63,64] These experimental results indicate that our designed all-in-one PBSIL semi-solid polymer electrolyte can achieve excellent cycling performance in LMBs equipped with various cathode materials, highlighting its versatility and effectiveness in enhancing the robustness and longevity of LMBs across different operational settings.

Both coin and pouch Li‖NCM811 full cells were assembled to evaluate the practical electrochemical performance and safety of the all-in-one PBSIL electrolyte. The full coin cells (a low N/P ratio of 3) with thin Li foil (20 μm) and high-loading NCM811 cathodes (8 mg cm^{-2}) deliver a stable cycling performance over 100 cycles with a discharge capacity of 163 mA h g^{-1} at 0.1C (Fig. 5a). Meanwhile, the pouch cells display a high discharge capacity of 188 mA h g^{-1} at 0.2C with an exceptional capacity retention of 99% over 60 cycles (Fig. 5b). Furthermore, the semi-solidstate cylindrical and multi-layer pouch cells were assembled to further explore the compatibility of PBSIL with conventional winding and *Z*-stacking process (Scheme 1, Fig. 5c, f, and Tables S3, S4, ESI†). The PBSIL-based cylindrical LMB can be successfully operated at 25 °C, delivering a discharge capacity of 109 mA h at 0.05C (Fig. 5e), marking the first instance of a free-standing PE being implemented in practical cylindrical LMBs at ambient temperature. Additionally, leveraging its superior mechanical property, PBSIL has been utilized to assemble a multi-layer pouch cell using *Z*-stacking process (Fig. 5f). This pouch cell was successfully used to power a mobile phone (Fig. 5g), exhibiting a discharge capacity of 69 mA h at 0.05C (Fig. 5h). These results demonstrate immense

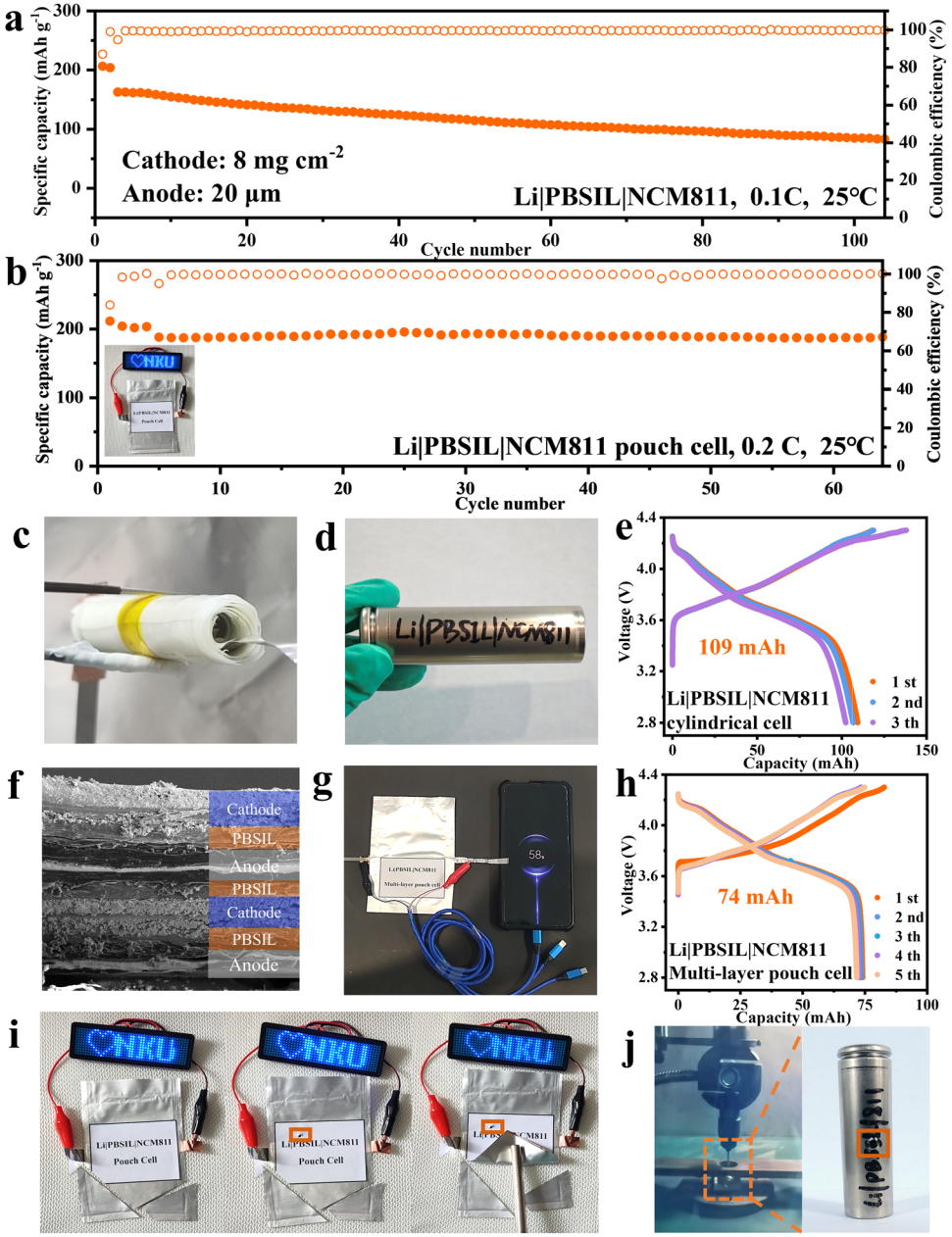

Fig. 5 (a) Cycling performances of 20 μm Li|PBSIL|8 mg cm^{-2} NCM811 coin cell at 0.1C. (b) Cycling performance of Li|PBSIL|NCM811 pouch cell. (c) and (d) Optical images of cylindrical cell. (e) Charge–discharge profiles of cylindrical cell. (f) Cross-sectional SEM image of Li|PBSIL|NCM811 multi-layer pouch cell. (g) Optical image of the pouch cell charging a phone. (h) Charge–discharge profiles of the pouch cell. (i) Optical images of pouch cell powering a light-emitting diode screen under harsh conditions including bending, cutting and punching. (j) Optical images of cylindrical cell during the nail penetration test.

potential of PBSIL in industrial applications. To further evaluate the safety of the PBSIL electrolyte, a Li|PBSIL|NCM811 pouch cell was assembled to power a light-emitting diode (LED) screen with an NKU logo, and it demonstrated stable operation even under harsh conditions (Fig. 5i). Simultaneously, an industry-level nail penetration test with more stringent conditions was carried out using PBSIL-based cylindrical LMB. The test showed no evident sign of smoking or combustion, which indicated the excellent safety of our PBSIL system (Fig. 5j and Video S1, ESI†). Therefore, our developed all-in-one PBSIL, characterized by its outstanding industrial compatibility, safety, and electrochemical performance, would satisfy the requirements of true industrial roll-to-roll mass production of LMBs.

3. Conclusion

We have developed a roll-to-roll processable, all-in-one single-ion conducting semi-solid polymer electrolyte (PBSIL) by fine-tuning Li^+ transport and anion immobilization through the

synergistic interaction of anion acceptor and solvate ionic liquid. This synergy confers PBSIL with restricted anion migration, weakened Li^+-$TFSI^-$ interaction, enhanced Li^+ transport kinetics, and a wide electrochemical window. Consequently, PBSIL achieves a high ionic conductivity (up to 9.2×10^{-4} S cm^{-1}) at 25 °C, a high Li^+ transference number (up to 0.86), and a high oxidation potential (5.3 V *vs.* Li/Li^+). Additionally, PBSIL's excellent compatibility with Li metal electrodes promotes uniform Li deposition and effectively inhibits Li dendrite growth, which contributes to the outstanding cycling performance of Li‖Li symmetric cells for over 3100 hours. Moreover, Li|PBSIL|NCM811 cells exhibit ultra-long cycling performance over 1300 cycles with an impressive capacity retention of 75%, positioning them among the top-performing free-standing PEs. Furthermore, this study marks the first successful implementation of free-standing PBSIL membranes in semi-solid state cylindrical and *Z*-stacked pouch cells at ambient temperature. Thus, our work presents an effective chemical regulation strategy and scalable design approach for PEs, demonstrating its significant potential for development in long-cycling LMBs.

Author contributions

Jinping Zhang: conceptualization, validation, formal analysis, investigation, data curation, writing – original draft, writing – review & editing. Jie Zhu: conceptualization, validation, formal analysis, investigation. Ruiqi Zhao: formal analysis. Jie Liu: formal analysis. Xingchen Song: formal analysis. Nuo Xu: formal analysis. Yansong Liu: formal analysis. Hongtao Zhang: conceptualization, supervision, writing – review & editing. Xiangjian Wang: supervision, formal analysis. Yanfeng Ma: supervision, formal analysis. Chenxi Li: supervision, formal analysis. Yongsheng Chen: conceptualization, validation, formal analysis, data curation, resources, writing – review & editing, supervision, project administration, funding acquisition.

Data availability

The data supporting this article have been included as part of the ESI.†

Conflicts of interest

The authors declare no conflict of interest.

Acknowledgements

The authors gratefully acknowledge the financial support from National Natural Science Foundation of China (NSFC, 52090034), and the National Key R&D Program of China (2020YFA0711500).

References

1 A. Varzi, R. Raccichini, S. Passerini and B. Scrosati, *J. Mater. Chem. A*, 2016, **4**, 17251–17259.
2 H. P. Liang, M. Zarrabeitia, Z. Chen, S. Jovanovic, S. Merz, J. Granwehr, S. Passerini and D. Bresser, *Adv. Energy Mater.*, 2022, **12**, 2200013.
3 M. A. Cabañero Martínez, N. Boaretto, A. J. Naylor, F. Alcaide, G. D. Salian, F. Palombarini, E. Ayerbe, M. Borras and M. Casas-Cabanas, *Adv. Energy Mater.*, 2022, **12**, 2201264.
4 Q. Zhou, J. Ma, S. Dong, X. Li and G. Cui, *Adv. Mater.*, 2019, **31**, 1902029.
5 A. Manthiram, X. Yu and S. Wang, *Nat. Rev. Mater.*, 2017, **2**, 16103.
6 J. Schnell, T. Günther, T. Knoche, C. Vieider, L. Köhler, A. Just, M. Keller, S. Passerini and G. Reinhart, *J. Power Sources*, 2018, **382**, 160–175.
7 L.-Z. Fan, H. He and C.-W. Nan, *Nat. Rev. Mater.*, 2021, **6**, 1003–1019.
8 R. Schröder, M. Aydemir and G. Seliger, *Procedia Manuf.*, 2017, **8**, 104–111.
9 L. Xu, Y. Lu, C. Z. Zhao, H. Yuan, G. L. Zhu, L. P. Hou, Q. Zhang and J. Q. Huang, *Adv. Energy Mater.*, 2020, **11**, 2002360.
10 X. Lu, Y. Wang, X. Xu, B. Yan, T. Wu and L. Lu, *Adv. Energy Mater.*, 2023, **13**, 2301746.
11 D. Zhou, D. Shanmukaraj, A. Tkacheva, M. Armand and G. Wang, *Chem*, 2019, **5**, 2326–2352.
12 K. Wen, C. Xin, S. Guan, X. Wu, S. He, C. Xue, S. Liu, Y. Shen, L. Li and C. W. Nan, *Adv. Mater.*, 2022, **34**, 2202143.
13 C. Wang, H. Liu, Y. Liang, D. Li, X. Zhao, J. Chen, W. Huang, L. Gao and L. Z. Fan, *Adv. Funct. Mater.*, 2022, **33**, 2209828.
14 K. Dai, C. Ma, Y. M. Feng, L. J. Zhou, G. C. Kuang, Y. Zhang, Y. Q. Lai, X. W. Cui and W. F. Wei, *J. Mater. Chem. A*, 2019, **7**, 18547–18557.
15 K. R. Deng, D. M. Han, S. Ren, S. J. Wang, M. Xiao and Y. Z. Meng, *J. Mater. Chem. A*, 2019, **7**, 13113–13119.
16 S. S. Chen, Y. Li, Y. Wang, Z. Y. Li, C. Peng, Y. Y. Feng and W. Feng, *Macromolecules*, 2021, **54**, 9135–9144.
17 D. Zhou, A. Tkacheva, X. Tang, B. Sun, D. Shanmukaraj, P. Li, F. Zhang, M. Armand and G. X. Wang, *Angew. Chem., Int. Ed.*, 2019, **58**, 6001–6006.
18 J. Zhu, Z. Zhang, S. Zhao, A. S. Westover, I. Belharouak and P. F. Cao, *Adv. Energy Mater.*, 2021, **11**, 2003836.
19 Y. Nie, T. Yang, D. Luo, Y. Liu, Q. Ma, L. Yang, Y. Yao, R. Huang, Z. Li, E. M. Akinoglu, G. Wen, B. Ren, N. Zhu, M. Li, H. Liao, L. Tan, X. Wang and Z. Chen, *Adv. Energy Mater.*, 2023, **13**, 2204218.
20 C. Zhang, Z. Lu, M. Song, Y. Zhang, C. Jing, L. Chen, X. Ji and W. Wei, *Adv. Energy Mater.*, 2023, **13**, 2203870.
21 L. Yang, Y. X. Huang, M. K. Tufail, X. F. Wang and W. Yang, *Small*, 2022, **18**, 2202060.
22 J. M. Du, X. R. Duan, W. Y. Wang, G. C. Li, C. H. Li, Y. C. Tan, M. T. Wan, Z. W. Seh, L. Wang and Y. M. Sun, *Nano Lett.*, 2023, **23**, 3369–3376.
23 S. Y. Yuan, J. L. Bao, J. S. Wei, Y. Y. Xia, D. G. Truhlar and Y. G. Wang, *Energy Environ. Sci.*, 2019, **12**, 2741–2750.
24 H. T. T. Nguyen, D. H. Nguyen, Q. C. Zhang, V. C. Nguyen, Y. L. Lee, J. S. Jan and H. Teng, *Adv. Funct. Mater.*, 2023, **33**, 2213469.

25 R. Bouchet, S. Maria, R. Meziane, A. Aboulaich, L. Lienafa, J.-P. Bonnet, T. N. T. Phan, D. Bertin, D. Gigmes, D. Devaux, R. Denoyel and M. Armand, *Nat. Mater.*, 2013, **12**, 452–457.
26 C. Cao, Y. Li, S. Chen, C. Peng, Z. Li, L. Tang, Y. Feng and W. Feng, *ACS Appl. Mater. Interfaces*, 2019, **11**, 35683–35692.
27 H. Yuan, J. Luan, Z. Yang, J. Zhang, Y. Wu, Z. Lu and H. Liu, *ACS Appl. Mater. Interfaces*, 2020, **12**, 7249–7256.
28 X. Lin, J. Yu, M. B. Effat, G. Zhou, M. J. Robson, S. C. T. Kwok, H. Li, S. Zhan, Y. Shang and F. Ciucci, *Adv. Funct. Mater.*, 2021, **31**, 2010261.
29 T. Tamura, K. Yoshida, T. Hachida, M. Tsuchiya, M. Nakamura, Y. Kazue, N. Tachikawa, K. Dokko and M. Watanabe, *Chem. Lett.*, 2010, **39**, 753–755.
30 K. Yoshida, M. Tsuchiya, N. Tachikawa, K. Dokko and M. Watanabe, *J. Phys. Chem. C*, 2011, **115**, 18384–18394.
31 Y. Yuan, X. Peng, B. Wang, K. Xue, Z. Li, Y. Ma, B. Zheng, Y. Song and H. Lu, *J. Mater. Chem. A*, 2023, **11**, 1301–1311.
32 S. Chereddy, J. Aguirre, D. Dikin, S. L. Wunder and P. R. Chinnam, *ACS Appl. Energy Mater.*, 2019, **3**, 279–289.
33 Y. Kitazawa, K. Iwata, S. Imaizumi, H. Ahn, S. Y. Kim, K. Ueno, M. J. Park and M. Watanabe, *Macromolecules*, 2014, **47**, 6009–6016.
34 Y. Kitazawa, K. Iwata, R. Kido, S. Imaizumi, S. Tsuzuki, W. Shinoda, K. Ueno, T. Mandai, H. Kokubo, K. Dokko and M. Watanabe, *Chem. Mater.*, 2017, **30**, 252–261.
35 Z. E. Liu, Z. W. Hu, X. A. Jiang, X. W. Wang, Z. Li, Z. J. Chen, Y. Zhang and S. G. Zhang, *Small*, 2022, **18**, 2203011.
36 F. Tao, X. Wang, S. Jin, L. Tian, Z. Liu, X. Kang and Z. Liu, *Adv. Mater.*, 2023, **35**, 2300687.
37 H. Zhang, C. M. Li, M. Piszcz, E. Coya, T. Rojo, L. M. Rodriguez-Martinez, M. Armand and Z. B. Zhou, *Chem. Soc. Rev.*, 2017, **46**, 797–815.
38 K. R. Deng, T. Y. Guan, F. H. Liang, X. Q. Zheng, Q. G. Zeng, Z. Liu, G. X. Wang, Z. P. Qiu, Y. F. Zhang, M. Xiao, Y. Z. Meng and L. Wei, *J. Mater. Chem. A*, 2021, **9**, 7692–7702.
39 G. Chen, C. Niu, X. Liao, Y. Chen, W. Shang, J. Du and Y. Chen, *Solid State Ionics*, 2020, **349**, 115309.
40 T. Li, X. Q. Zhang, N. Yao, Y. X. Yao, L. P. Hou, X. Chen, M. Y. Zhou, J. Q. Huang and Q. Zhang, *Angew. Chem., Int. Ed.*, 2021, **60**, 22683–22687.
41 Y. Han, Y. Zhou, J. Zhu, Z. Sun, L. Xu, C. Li, Y. Ma, H. Zhang and Y. Chen, *Sci. China Mater.*, 2020, **63**, 2344–2350.
42 S. Xia, B. Yang, H. Zhang, J. Yang, W. Liu and S. Zheng, *Adv. Funct. Mater.*, 2021, **31**, 2101168.
43 Y. Cheng, X. Liu, Y. Guo, G. Dong, X. Hu, H. Zhang, X. Xiao, Q. Liu, L. Xu and L. Mai, *Adv. Mater.*, 2023, **35**, 2303226.
44 J. Zhu, J. P. Zhang, R. Q. Zhao, Y. Zhao, J. Liu, N. Xu, X. J. Wan, C. X. Li, Y. F. Ma, H. T. Zhang and Y. S. Chen, *Energy Storage Mater.*, 2023, **57**, 92–101.
45 H. Li, Y. Du, X. Wu, J. Xie and F. Lian, *Adv. Funct. Mater.*, 2021, 2103049.
46 X. S. Ge, F. C. Song, A. B. Du, Y. J. Zhang, B. Xie, L. Huang, J. W. Zhao, S. M. Dong, X. H. Zhou and G. L. Cui, *Adv. Energy Mater.*, 2022, **12**, 2201464.
47 Z. W. Cheng, T. Liu, B. Zhao, F. Shen, H. Y. Jin and X. G. Han, *Energy Storage Mater.*, 2021, **34**, 388–416.
48 S. J. Wen, C. Luo, Q. R. Wang, Z. Y. Wei, Y. X. Zeng, Y. D. Jiang, G. Z. Zhang, H. L. Xu, J. Wang, C. Y. Wang, J. Chang and Y. H. Deng, *Energy Storage Mater.*, 2022, **47**, 453–461.
49 Z. Li, R. Yu, S. T. Weng, Q. H. Zhang, X. F. Wang and X. Guo, *Nat. Commun.*, 2023, **14**, 482.
50 J. C. Guo, S. J. Tan, C. H. Zhang, W. P. Wang, Y. Zhao, F. Y. Wang, X. S. Zhang, R. Wen, Y. Zhang, M. Fan, S. Xin, J. Zhang and Y. G. Guo, *Adv. Mater.*, 2023, **35**, 2300350.
51 C. Zhang, J. Xie, C. Zhao, Y. Yang, Q. An, Z. Mei, Q. Xu, Y. Ding, G. Zhao and H. Guo, *Adv. Mater.*, 2023, **35**, 2304511.
52 S. Y. Li, Q. L. Liu, W. D. Zhang, L. Fan, X. Y. Wang, X. Wang, Z. Y. Shen, X. X. Zang, Y. Zhao, F. Y. Ma and Y. Y. Lu, *Adv. Sci.*, 2021, **8**, 2003240.
53 W. D. Zhang, Q. Wu, J. X. Huang, L. Fan, Z. Y. Shen, Y. He, Q. Feng, G. N. Zhu and Y. Y. Lu, *Adv. Mater.*, 2020, **32**, 2001740.
54 Z. Yu, P. E. Rudnicki, Z. W. Zhang, Z. J. Huang, H. Celik, S. T. Oyakhire, Y. L. Chen, X. Kong, S. C. Kim, X. Xiao, H. S. Wang, Y. Zheng, G. A. Kamat, M. S. Kim, S. F. Bent, J. Qin, Y. Cui and Z. N. Bao, *Nat. Energy*, 2022, **7**, 94–106.
55 A. Abouimrane, J. Ding and I. J. Davidson, *J. Power Sources*, 2009, **189**, 693–696.
56 J. Kalhoff, D. Bresser, M. Bolloli, F. Alloin, J. Y. Sanchez and S. Passerini, *ChemSusChem*, 2014, **7**, 2939–2946.
57 Q. F. Zheng, Y. Yamada, R. Shang, S. Ko, Y. Y. Lee, K. Kim, E. Nakamura and A. Yamada, *Nat. Energy*, 2020, **5**, 291–298.
58 Q. F. Sun, S. Wang, Y. Ma, D. W. Song, H. Z. Zhang, X. X. Shi, N. Zhang and L. Q. Zhang, *Adv. Mater.*, 2023, **35**, 2300998.
59 Y. Chen, Z. Yu, P. Rudnicki, H. Gong, Z. Huang, S. C. Kim, J. C. Lai, X. Kong, J. Qin, Y. Cui and Z. Bao, *J. Am. Chem. Soc.*, 2021, **143**, 18703–18713.
60 J. Zhu, R. Zhao, J. Zhang, X. Song, J. Liu, N. Xu, H. Zhang, X. Wan, X. Ji, Y. Ma, C. Li and Y. Chen, *Angew. Chem., Int. Ed.*, 2024, **63**, 202400303.
61 Y. Guo, S. Pan, X. Yi, S. Chi, X. Yin, C. Geng, Q. Yin, Q. Zhan, Z. Zhao, F. M. Jin, H. Fang, Y. B. He, F. Kang, S. Wu and Q. H. Yang, *Adv. Mater.*, 2024, **36**, 2308493.
62 W. Zhang, V. Koverga, S. Liu, J. Zhou, J. Wang, P. Bai, S. Tan, N. K. Dandu, Z. Wang, F. Chen, J. Xia, H. Wan, X. Zhang, H. Yang, B. L. Lucht, A.-M. Li, X.-Q. Yang, E. Hu, S. R. Raghavan, A. T. Ngo and C. Wang, *Nat. Energy*, 2024, **9**, 386–400.
63 R. Q. Zhao, M. M. Wu, P. X. Jiao, X. T. Wang, J. Zhu, Y. Zhao, H. T. Zhang, K. Zhang, C. X. Li, Y. F. Ma and Y. S. Chen, *Nano Res.*, 2023, **16**, 6805–6814.
64 L. Xu, Z. Sun, Y. Zhu, Y. Han, M. Wu, Y. Ma, Y. Huang, H. Zhang and Y. Chen, *Sci. China Mater.*, 2020, **63**, 2435–2442.

